The Astrophysical Journal, 784:155 (13pp), 2014 April 1 doi:10.1088/0004-637X/784/2/155

A LOW-ORDER MODEL OF WATER VAPOR, CLOUDS, AND THERMAL EMISSION FOR TIDALLY LOCKED TERRESTRIAL PLANETS

Jun Yang and Dorian S. Abbot
Department of the Geophysical Sciences, University of Chicago, 5734 South Ellis Avenue, Chicago, IL 60637, USA; junyang28@uchicago.edu
Received 2013 December 5; accepted 2014 February 17; published 2014 March 18

ABSTRACT

In the spirit of minimal modeling of complex systems, we develop an idealized two-column model to investigate the climate of tidally locked terrestrial planets with Earth-like atmospheres in the habitable zone of M-dwarf stars. The model is able to approximate the fundamental features of the climate obtained from three-dimensional (3D) atmospheric general circulation model (GCM) simulations. One important reason for the two-column model's success is that it reproduces the high cloud albedo of the GCM simulations, which reduces the planet's temperature and delays the onset of a runaway greenhouse state. The two-column model also clearly illustrates a secondary mechanism for determining the climate: the nightside acts as a "radiator fin" through which infrared energy can be lost to space easily. This radiator fin is maintained by a temperature inversion and dry air on the nightside, and plays a similar role to the subtropics on modern Earth. Since one-dimensional radiative–convective models cannot capture the effects of the cloud albedo and radiator fin, they are systematically biased toward a narrower habitable zone. We also show that cloud parameters are the most important in the two-column model for determining the day–night thermal emission contrast, which decreases and eventually reverses as the stellar flux increases. This reversal is important because it could be detected by future extrasolar planet characterization missions, which would suggest that the planet has Earth-like water clouds and is potentially habitable.

Key words: astrobiology – planets and satellites: atmospheres – planets and satellites: detection – stars: low-mass

Online-only material: color figures

1. INTRODUCTION

Extrasolar planets in tidally locked orbital configurations around low-mass and relatively cool M-dwarf stars are the prime targets of several ongoing and proposed planet search programs (Tarter et al. 2007). In advance of direct observations of these planets, numerical models, including both single column radiative–convective models (e.g., Kasting et al. 1993; Wordsworth et al. 2010; Hu & Ding 2011; Kopparapu et al. 2013) and three-dimensional (3D) atmospheric general circulation models (GCMs; Joshi et al. 1997; Joshi 2003; Merlis & Schneider 2010; Heng & Vogt 2011; Pierrehumbert 2011; Edson et al. 2011; Wordsworth et al. 2011; Leconte et al. 2013; Shields et al. 2013; Yang et al. 2013, hereafter, YCA13) have been employed to investigate their potential climates. Radiative–convective models employ sophisticated radiative schemes, but neglect atmospheric dynamics. GCMs calculate atmospheric dynamics in detail and use radiative schemes of varying levels of complexity.

In addition to numerically intensive modeling, idealized models can help make clear essential physical mechanisms in complex systems such as the climates of tidally locked planets. Low-order models are relatively easy to analyze and determine the dominant mechanisms, since mechanisms can be easily added, removed, or changed. They can be compared with more complex models to aid the interpretation of complex model results, and they help to address the critical question of what is the minimum physics necessary to understand a particular problem.

In this study, we develop a two-column model of the atmospheres of Earth-like tidally locked planets in order to better understand the following two questions: (1) what determines the surface temperature? and (2) what determines the thermal infrared emission contrast between dayside and nightside? These questions are critical because the surface temperature determines whether liquid water can be maintained on the surface, which determines habitability in the traditional sense, and the thermal emission contrast will be one of the first observational signals that will be used to characterize tidally locked terrestrial planets (e.g., Knutson et al. 2007).

The model divides the atmosphere into two columns with one representing the dayside and the other representing the nightside (Figure 1). This is the most basic possible simplification that allows horizontal heterogeneity, and it is justified by the following facts: (1) only the dayside receives stellar flux from the parent star, whereas the nightside is heated by atmospheric and ocean heat import from the dayside. The temperatures of the two sides are therefore determined by distinct physical processes. (2) GCM simulations have found that on the nightside, horizontal surface and air temperature gradients are extremely small and atmospheric descent occurs throughout the nightside (Joshi et al. 1997; Merlis & Schneider 2010); therefore, the nightside atmosphere can be approximated as a single column. (3) On the dayside, the surface temperature is homogeneous in the vicinity of the substellar point in GCM simulations, and more broadly, much of the dayside is characterized by robust moist convection and mean ascent (YCA13; Merlis & Schneider 2010), so that it can be roughly treated as a single column. (4) The dayside has a moist atmosphere with a robust hydrological cycle whereas the nightside atmosphere is extremely dry (Merlis & Schneider 2010; Edson et al. 2011). (5) Future observations of horizontal variations in the climate on tidally locked terrestrial planets are likely to be coarse, so it is reasonable to develop a model with minimal horizontal resolution.

In our model, the dayside column is thought of as a moist region with deep convection, mean ascent, and a warm surface. The air temperature follows a saturation moist adiabatic temperature profile. In this way the dayside is similar to the warm

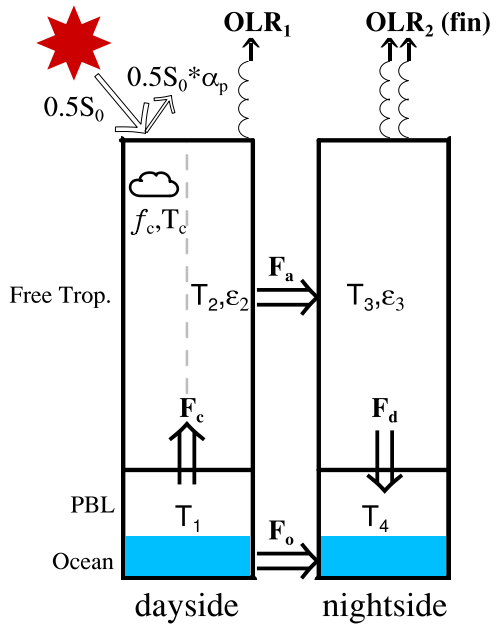

Figure 1. Schematic representation of the two-column model for the climate of tidally locked terrestrial planets. The dayside column consists of a cloudy part and a clear-sky part. S_0: stellar flux at substellar point; α_p: planetary albedo; OLR: outgoing longwave radiation (infrared emission to space); f_c: effective cloud fraction; T_c: cloud emission temperature; $\varepsilon_{2,3}$: atmospheric emissivity; PBL: planetary boundary layer; F_c: convective heat flux; F_a: atmospheric heat transport from dayside to nightside; F_o: ocean heat transport; and F_d: the fraction of atmospheric heat transport from the dayside to the nightside deposited in the nightside boundary layer due to adiabatic heating.

(A color version of this figure is available in the online journal.)

pool of the tropical Pacific Ocean on Earth, where the temperature profile is close to a moist adiabat (Xu & Emanuel 1989). The nightside column has mean descent with dry air and a cold surface, which is analogous in some ways to the subtropics of Earth. The implicit atmospheric circulation connecting the dayside and the nightside in the model approximates a global-scale Walker circulation driven by the stellar energy contrast, as obtained in GCM simulations (see the review of Showman et al. 2013). To simulate the effect of clouds, we employ a simple convective cloud scheme and tune one free parameter of the scheme to produce a similar cloud albedo to that obtained in the GCM simulations of YCA13. At a given stellar flux and a specified ocean heat transport, the model computes dayside and nightside surface temperature, dayside and nightside free-tropospheric temperature, dayside convective heat flux, and atmospheric heat transport from the dayside to the nightside.

Similar types of models have been employed to investigate the climate of the tropics on modern Earth. Such models have been found to be useful for identifying the mechanisms that regulate the surface temperature of the tropical Pacific Ocean, including surface evaporation (Hartmann & Michelsen 1993), convective clouds (Ramanathan & Collins 1991), stratus low clouds (Larson et al. 1999), water vapor greenhouse effect (Pierrehumbert 1995), horizontal atmospheric heat transport (Hartmann & Michelsen 1993; Pierrehumbert 1995), and ocean dynamics (e.g., Clement & Seager 1999). Because of the extreme simplifications of these column models, their applicability to direct comparison with detailed and spatially dense observations is somewhat limited; however, they have significantly improved our understanding of tropical climate by helping to identify the essential processes that govern the system.

We tune our two-column model to a GCM, which fully resolves atmospheric circulation, radiative transfer, the hydrological cycle, and clouds. We use an Earth GCM, the Community Atmosphere Model version 3 (CAM3; Collins et al. 2004), developed by the National Center for Atmospheric Research. The GCM is coupled to a mixed layer ocean with a uniform depth of 50 m. We have modified the GCM to simulate the climate of tidally locked planets around M stars (for details, see YCA13). The default planetary radius, gravity, and rotation period are set to two times Earth's, 13.7 m s^{-2}, and 60 Earth-days, respectively. The atmosphere is composed of N_2 and H_2O with a surface pressure of 1 bar, and other greenhouse gases such as CO_2, CH_4, N_2O, and O_3 are set to zero. Three groups of experiments with different stellar fluxes (from 1000 to 2400 W m^{-2}), ocean heat transport (from 0 to 55 W m^{-2}), and rotation periods (from 5 to 100 Earth-days) were performed, and the results are used here for comparisons with the two-column model. The GCM and the two-column model share the same planetary and atmospheric parameters, such as planetary gravity and specific heat of air.

The goal of this study is to increase understanding of the key controls on surface temperature and thermal emission flux of tidally locked Earth-like planets. The basic physical processes that we build into the model are outlined in Section 2. The model is developed in Section 3. Section 4 presents the behavior of the two-column model, comparisons of model results with GCM simulations, and sensitivity analyses of the model. In Section 5, the critical stellar flux at which the day–night thermal emission contrast becomes negative is addressed. This contrast is essential for the interpretation of phase curves of terrestrial planets that will be measured in the near future. Section 6 summarizes the main findings of this study.

2. ESSENTIAL PHYSICAL PROCESSES

The orbital distance of tidally locked planets in the habitable zone of M stars should be in the range of ≈0.02–0.2 AU (1 AU is the distance between Earth and Sun; YCA13; Kasting et al. 1993; Kopparapu et al. 2013), corresponding to rotation periods of tens of Earth days. The extreme variation in stellar radiation around the planet and the slow rotation rate (corresponding to a weak Coriolis force) imply that in many ways the climate of tidally locked planets will be quite different from that of Earth. Despite this, we should still be able to use basic principles of climate dynamics discovered by studying Earth to better understand the climate of these planets. In this section, we outline the essential physical mechanisms that we believe govern the climate of tidally locked terrestrial planets, including the weak-temperature-gradient (WTG) approximation, a stabilizing cloud feedback, and the fixed anvil temperature (FAT) hypothesis. We will also discuss the factors determining thermal emission to space.

2.1. The Weak-temperature-gradient Approximation

GCM simulations suggest that the free-tropospheric temperature of tidally locked habitable planets should be quite horizontally uniform (Figure 2(a)) due to the weak Coriolis force. This property is similar to the condition of the tropics on Earth (Pierrehumbert 1995; Sobel et al. 2001) where the Coriolis force is also weak, which allows the horizontal temperature gradients of the free troposphere to be approximated as zero. This is referred to as the WTG approximation. It is important to note that the WTG approximation only applies to the atmosphere above

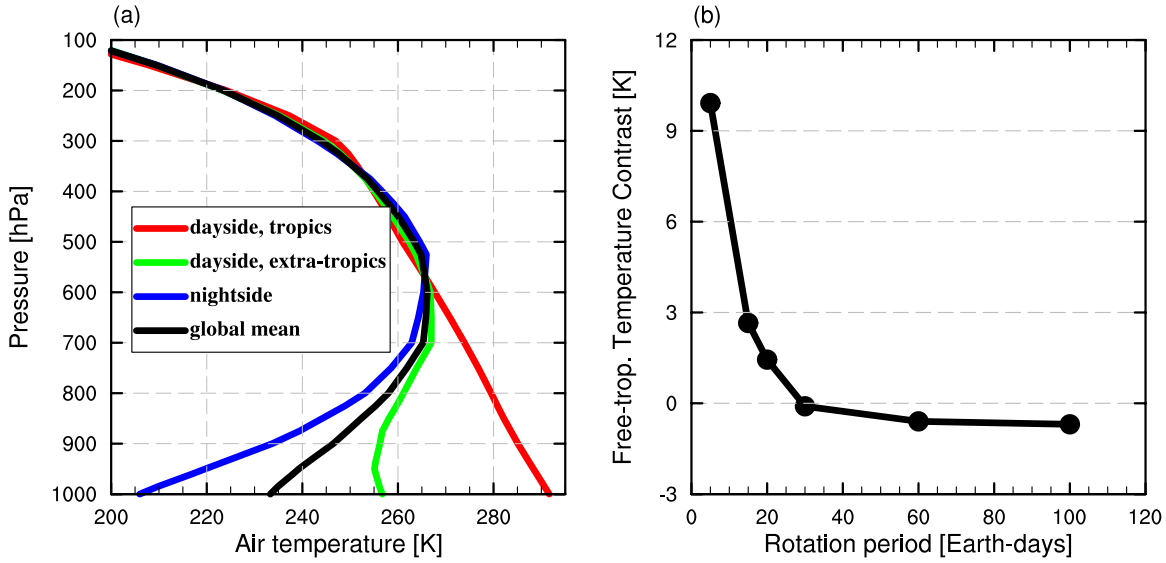

Figure 2. GCM output that supports the WTG approximation for tidally locked planets. (a) Vertical temperature profiles for a tidally locked configuration with a rotation period of 60 Earth days. Red line: for the tropics (30°S–30°N) of the dayside; green line: for the extra-tropics of the dayside; blue line: for the entire nightside; and black line: global mean. (b) Free-tropospheric temperature contrast between dayside and nightside (mean value between the pressure levels of 100 and 600 hPa) as a function of rotation period. The stellar flux is 1200 W m^{-2} in these simulations.

(A color version of this figure is available in the online journal.)

the planetary boundary layer. In the planetary boundary layer, where frictional forces become important in the momentum balance, horizontal temperature gradients can remain large, so that the nightside surface can become much colder than the dayside surface. On a tidally locked planet, where strong inversions develop on the nightside and at high latitudes on the dayside, a stably stratified planetary boundary layer can extend up to ≈600 hPa (see Figure 2(a)). Nevertheless, a model approximating the atmosphere with just two levels, the boundary layer (and surface) and the free troposphere, can yield a faithful representation of the longitudinal variation in infrared emission to space (Mills & Abbot 2013).

The WTG in the free troposphere can be brought about by a variety of physical processes. Temperature gradients set up gravity waves that quickly diminish them. Additionally, the atmospheric circulation of tidally locked planets is characterized by a global-scale Walker circulation: strong updrafts near the substellar point, divergence at high altitudes, broad downwelling at the entire nightside, and convergence flows at low altitudes, returning to the substellar region (Showman et al. 2013). Moreover, the zonal-mean zonal wind velocity is dominated by a weak eastward superrotation along the equator. This equatorial superrotation results from equatorward zonal momentum transport by Rossby waves induced by strong zonal variations in the stellar radiation (e.g., Showman & Polvani 2011). All of these processes are important for transporting heat from dayside to nightside and maintaining the WTG in the troposphere.

The WTG approximation is not valid if the timescale for atmospheric heat transport is longer than the radiative timescale. Two ways for this to happen are if the planet has a small orbital (and rotational) period or has an extremely hot and/or thin atmosphere (Perez-Becker & Showman 2013). For our sample GCM simulations the largest horizontal temperature differences in the free troposphere around the planet are only ≈10 K when the orbital period is 5 Earth days (Figure 2(b)). This is consistent with previous work indicating that the WTG approximation does a good job of approximating the temperature profile of a tidally locked planet even if the rotation period is only 1 Earth day (Merlis & Schneider 2010; Mills & Abbot 2013), and suggests that the WTG approximation may be more broadly applicable than one might initially suspect.

2.2. The Stabilizing Cloud Feedback

Clouds contribute most of the planetary albedo of Earth (Donohoe & Battisti 2011). Consistent with the global-scale Walker circulation and ascent at the substellar region, most parts of the dayside of tidally locked Earth-like planets would be covered by water clouds (YCA13; Edson et al. 2011), which would greatly increase the planetary albedo and dramatically cool the planet. The cloud albedo effect becomes stronger as the planet is moved closer to its parent star because higher stellar insolation drives stronger convection, producing more clouds and increasing their optical depth. This stabilizing cloud feedback significantly delays the onset of a runaway greenhouse state as the stellar flux increases and therefore shifts the inner edge of the habitable zone substantially toward its star (YCA13).

In the two-column model, we parameterize convection as a vertical mixing of moist static energy (MSE) between the boundary layer and the free troposphere. Convection commences when the boundary-layer MSE exceeds the free-tropospheric saturation MSE (Raymond 1995). The cloud fraction and cloud albedo are assumed to be proportional to the logarithm of the convective heat flux, as suggested by observations of tropical convective clouds on Earth (Slingo 1980). The logarithmic formula connects the optical properties of clouds to the strength of convection, and enables the model to capture the effect of the stabilizing cloud feedback.

2.3. The Fixed Anvil Temperature Hypothesis

Studies of tropical anvil clouds on Earth suggest that their emission temperature is nearly constant as the climate changes. This is referred to as the FAT hypothesis (Hartmann & Larson 2002). Energy balance in the tropical troposphere is primarily between convective heating by latent heat release in regions of deep convection and radiative

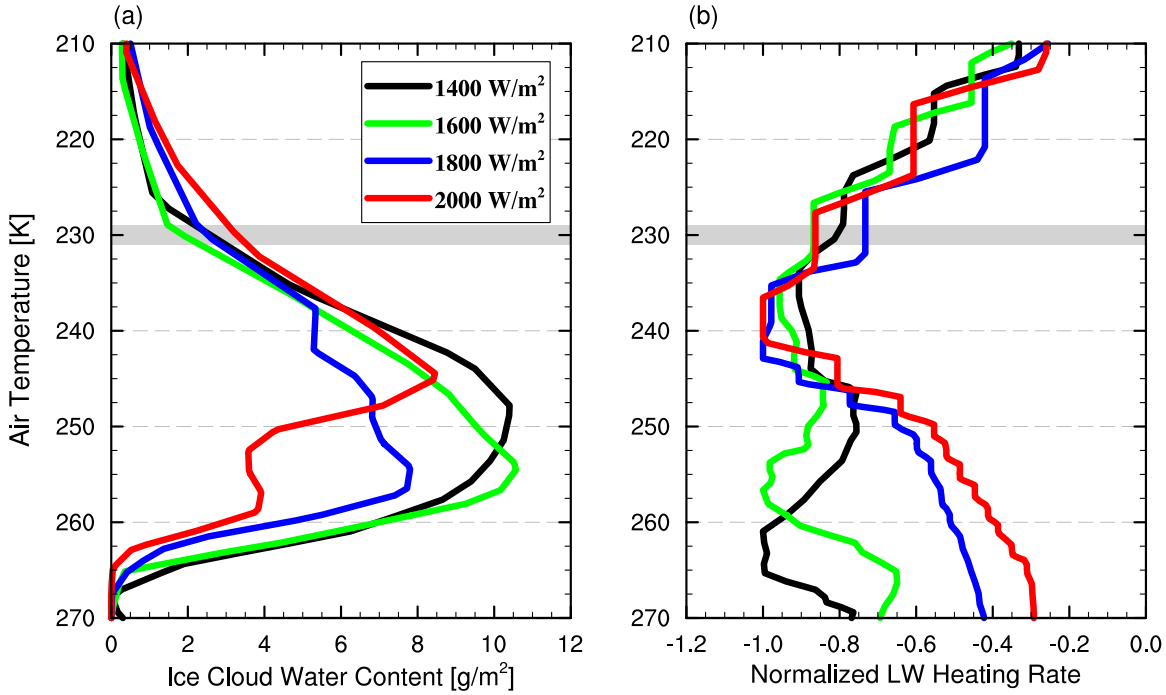

Figure 3. GCM output justifying the FAT hypothesis for tidally locked planets. (a) Dayside ice cloud water content and (b) normalized clear-sky longwave heating rate, as a function of air temperature. The horizontal gray bold line roughly shows the temperature at the top of ice clouds where a sharp decrease in the clear-sky longwave heating rate occurs. Note that the pressure at which $T = 230$ K occurs is ≈150, 100, 40, and 12 hPa for the stellar fluxes of 1400, 1600, 1800, and 2000 W m^{-2}, respectively.

(A color version of this figure is available in the online journal.)

cooling by longwave emission to space in clear-sky regions (i.e., the regions without clouds) with large-scale subsidence. Because of this, the detrainment level (where outflow occurs) of anvil clouds should be located at the altitude where the clear-sky radiative cooling diminishes rapidly. The clear-sky radiative cooling rate in the upper troposphere is primarily determined by water vapor emission. The temperature at which the saturation water vapor pressure becomes small enough that water vapor emission is ineffective is narrowly constrained by local air temperature because of the Clausius–Clapeyron relation, and does not depend on surface temperature. The FAT hypothesis asserts that the temperature at which anvil clouds detrain is determined by the level where a large decrease in water vapor radiative cooling occurs. According to the FAT hypothesis, the temperature at the top of anvil clouds should be nearly independent of surface temperature, which exerts a strong constraint on the strength of cloud longwave forcing.

Recent simulations with cloud-resolving models (e.g., Kuang & Hartmann 2007) and analyses with cloud object data (e.g., Li et al. 2012) support the FAT hypothesis. Furthermore, Zelinka & Hartmann (2010) show that the cloud-top temperature in GCMs with parameterized clouds also remain approximately constant as greenhouse gas concentrations are increased. Our GCM simulations of tidally locked planets also support the FAT hypothesis. As shown in Figure 3, the clear-sky cooling rate decreases rapidly at a constant air temperature, and the cloud-top temperature stays constant when the stellar flux is increased massively. In the two-column model, it is therefore reasonable to set the cloud-top temperature to a constant.

2.4. Factors Determining Thermal Emission to Space

A primary tool for deciphering the climate of terrestrial exoplanets will be to examine phase variations in their infrared emission flux, commonly referred to as outgoing longwave radiation (OLR) in Earth science. The OLR is primarily determined by surface temperature (T_s), air temperature (T_a), atmospheric specific humidity (q, the mass ratio of water vapor to dry air), and clouds. Changes in temperature and humidity have opposing effects on OLR: increases in T_s and T_a increase OLR, while increases in q decrease OLR due to the water vapor greenhouse effect (Pierrehumbert 2010). Clouds can also significantly reduce OLR (Ramanathan et al. 1989). OLR can be thought of as the sum of surface upward emission which survives absorption by water vapor, re-emission from the atmosphere, and a negative term due to cloud absorption,

$$\mathrm{OLR} = (1 - \varepsilon(q))\sigma T_s^4 + \varepsilon(q)\sigma T_a^4 - C_l, \quad (1)$$

where $\varepsilon(q)$ is the clear-sky atmospheric infrared emissivity as a function of specific humidity (q), C_l is the cloud longwave forcing (i.e., the change in OLR in the presence of clouds relative to the clear-sky condition), and σ is the Stefan–Boltzmann constant. For an optically thin clear-sky atmosphere, ε is close to zero, and OLR is close to the surface emission. For an optically thick clear-sky atmosphere, ε is close to one, and OLR is primarily determined by the emission from the upper levels of the atmosphere.

For tidally locked terrestrial planets, the dayside specific humidity tends to be higher than the nightside specific humidity at all atmospheric levels. This is because the relative humidity tends to be higher at all levels on the dayside, and additionally the dayside temperature is much higher in the boundary layer. As a result, the rate of increase of the dayside clear-sky OLR with stellar flux is much smaller than that on the nightside (Figure 4(a)). The high water vapor concentration shifts the atmospheric emission level to higher altitudes with colder temperatures, which keeps the dayside OLR from increasing much.

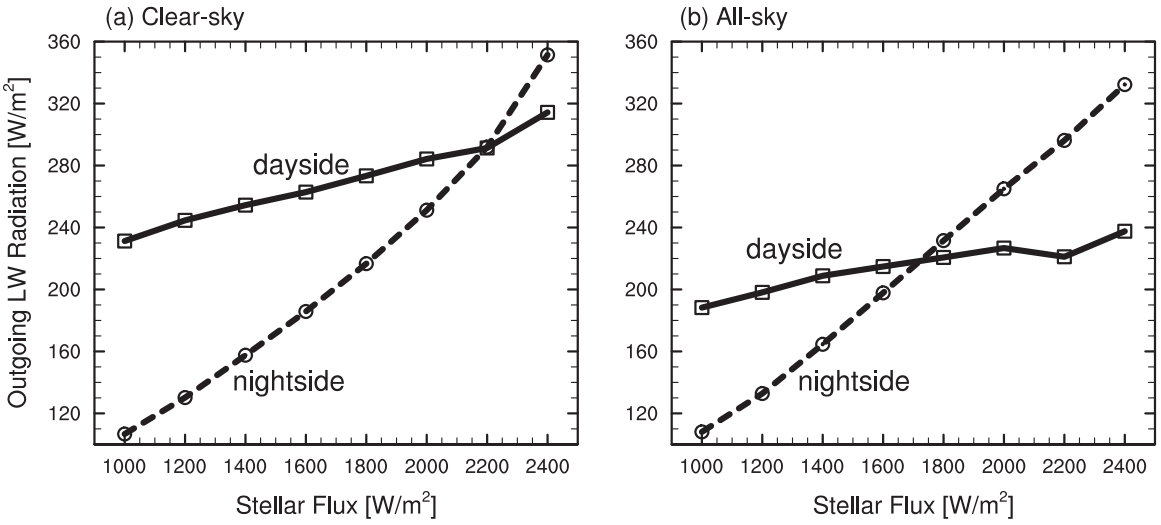

Figure 4. GCM simulated outgoing longwave radiation at the top of the atmosphere on the dayside (solid line) and on the nightside (dashed line) as a function of the stellar flux (S_0). (a) Clear-sky conditions without clouds and (b) all-sky conditions including the effect of clouds. Note: panels (a) and (b) are calculated with the same surface temperatures, air temperatures, and water vapor concentrations.

The dayside is covered by high-level clouds which strongly reduce the dayside OLR whereas the nightside is dominated by low-level clouds that have little effect on the nightside OLR. High-level clouds absorb thermal emission from the warm surface and reemit it to space following the Stefan–Boltzmann law at the temperature of the cloud, which is much lower than the surface temperature, reducing OLR. Low-level clouds have nearly zero effect on OLR because they have temperatures close to the surface temperature. GCM simulations show that as a result of the global circulation pattern, with ascent on the dayside and descent on the nightside, the dayside should be covered by both high-level and low-level clouds while the nightside should be dominated by low-level clouds (Figure 1 of YCA13) that form when water vapor is trapped in the boundary layer under the temperature inversion (see Figure 2(a)). Because of the combined effect of clouds and water vapor, the dayside all-sky (including clouds) OLR is nearly constant as the stellar flux is varied (Figure 4(b)).

In our two-column model, the clear-sky region of the atmosphere is treated as an equivalent gray gas atmosphere characterized by an emissivity that is a function of water vapor content (Pierrehumbert 2010). This representation qualitatively captures the greenhouse effect of water vapor without requiring detailed calculations of the radiative transfer. In order to calculate the cloud longwave forcing, the dayside column also includes a cloudy region that emits at a constant temperature (following the FAT hypothesis). This scheme does a reasonable job of simulating the cloud longwave effect.

3. THE TWO-COLUMN MODEL

In this section, we construct an idealized two-column model (shown schematically in Figure 1) that incorporates all the physical processes addressed in Section 2 above. The dayside column is thought of as a region with deep convection, net ascent, and a moist atmosphere. The nightside column has no convection and represents a dry region of mean descent. In each column, the upper level represents the free troposphere and the lower level represents both the boundary layer and the surface. The boundary layer and surface are assumed to be tightly coupled by turbulent mixing and therefore have approximately the same temperature. The dayside free troposphere has two parts, the clear-sky part and the cloudy part.

The model is formulated by requiring energy balance in the free troposphere and at the surface (Equations (2)–(5)), making the WTG approximation (Equation (6)), enforcing convective neutrality on the dayside (Equation (7)), and assuming the FAT hypothesis is correct (Equation (8)). The model equations are

$$\frac{1}{2}S_0(1-\alpha_p)-F_c-F_o+(1-f_c)\varepsilon_2\sigma T_2^4+f_c\sigma T_c^4-\sigma T_1^4=0, \quad (2)$$

$$F_c-F_a+(1-f_c)\varepsilon_2\sigma T_1^4+f_c\sigma T_1^4-2(1-f_c)\varepsilon_2\sigma T_2^4-2f_c\sigma T_c^4=0, \quad (3)$$

$$F_a-F_d+\varepsilon_3\sigma T_4^4-2\varepsilon_3\sigma T_3^4=0, \quad (4)$$

$$F_o+F_d+\varepsilon_3\sigma T_3^4-\sigma T_4^4=0, \quad (5)$$

$$T_2-T_3=0, \quad (6)$$

$$\mathrm{MSE}_1=\mathrm{MSE}_2^*, \quad (7)$$

$$T_c=230. \quad (8)$$

Here, T_1 and T_4 are the surface temperatures of the dayside and nightside, respectively; T_2 and T_3 are the free-tropospheric temperatures of the dayside and nightside, respectively; T_c is the cloud emission temperature; S_0 is the stellar flux at the substellar point and $(1/2)S_0$ is the stellar flux impinging on the dayside surface (averaged over the stellar zenith angle); α_p is the planetary albedo; F_c is the convective heat flux from the boundary layer to the free troposphere in the dayside column; F_a and F_o represent atmospheric and ocean heat transports from dayside to nightside, respectively; F_d is the adiabatic heating due to dry descent in the nightside column; ε_2 and ε_3 are the free tropospheric emissivities of the dayside and nightside, respectively; f_c is the effective cloud fraction; MSE_1 is the dayside surface MSE; and MSE_2^* is the dayside free-tropospheric saturation MSE. Using the six Equations (2)–(7), we are able to determine solutions for the six dependent variables of the model: surface temperature (T_1 and T_4), free-tropospheric temperature (T_2 and T_3), atmospheric heat transport (F_a), and dayside convective heat flux (F_c). This solution is a function of the independent variables: the strength of stellar flux (S_0), ocean heat transport (F_o), and model parameters.

Table 1
Model Parameters used for the Reference Climate Calculations

Parameter	Description	Value
P_a	Depth of convection	600 hPa
T_c	Cloud emission temperature	230 K
RH_1	Relative humidity of the dayside boundary layer	90%
RH_2	Relative humidity of the dayside free troposphere	80%
RH_3	Relative humidity of the nightside free troposphere	30%
k_1	Fraction of heat transport to the nightside deposited in the boundary layer (Equation (9))	0.2
k_2	Relates water vapor to the infrared opacity (Equation (10))	1000
k_3	Relates the strength of convection to the cloud fraction (Equation (13))	0.08

Following the WTG approximation, the atmospheric energy transport (F_a) is forced to be strong enough to drive the dayside and nightside free-tropospheric temperature together (Equation (6)). This approximation allows the details of atmospheric dynamics to be avoided but retains the net effect of atmospheric dynamics on the air temperature. We assume that some of F_a, the total atmospheric heat transport from the dayside to the nightside, is deposited in the boundary layer (F_d) and the rest is deposited in the free troposphere ($F_a - F_d$). We take F_d to be

$$F_d = k_1 F_a, \tag{9}$$

where k_1 is a constant parameter (see Table 1).

The surface and clouds are assumed to emit like blackbodies (i.e., $\varepsilon = 1$). The free troposphere is assumed to radiate as an equivalent gray body with emissivities of ε_2 and ε_3, determined by water vapor concentration,

$$\varepsilon_{2,3} = 1.0 - \exp\left(-\frac{\varkappa P_a}{g} q_{2,3}\right) = 1.0 - \exp(-k_2 q_{2,3}), \tag{10}$$

where q_2 and q_3 are specific humidities of the dayside and nightside respectively, $\varkappa$ is an absorption coefficient, q is the specific concentration of water vapor, P_a is the air pressure, and g is the acceleration due to gravity, and k_2 is a constant coefficient with $k_2 \equiv \varkappa P_a / g$. Equation (10) follows from the gray gas approximation (e.g., Pierrehumbert 2010), and is similar to that employed in Emanuel (2002). We calculate the specific humidity by assuming fixed relative humidities (RH_2 and RH_3, the ratio of water vapor partial pressure to saturation water vapor partial pressure) and calculating the saturation water vapor partial pressure using the Clausius–Clapeyron relationship. From the Clausius–Clapeyron relationship, saturation water vapor partial pressure is roughly exponential in air temperature, increasing ≈7% for each 1 K in temperature at Earth-like temperatures (Emanuel 1994). An additional term in Equation (10) could be easily added to account for the change of optical thickness due to atmospheric CO_2 absorption (for example, see Emanuel 2002).

The convective heat flux (F_c) is determined implicitly by requiring convective neutrality, which can be approximated by requiring that the boundary layer MSE equals the free-tropospheric saturation MSE (Abbot & Tziperman 2009). The MSE of the surface is

$$\mathrm{MSE}_1 = C_p T_1 + L q_1, \tag{11}$$

while the free-tropospheric saturation MSE is

$$\mathrm{MSE}_2^* = C_p T_2 + L q_2^* + g Z_a, \tag{12}$$

where C_p is the specific heat of the air at constant pressure ($C_p = 1005.7\ \mathrm{J\,kg^{-1}\,K^{-1}}$), L is the latent heat of evaporation ($L = 2.501 \times 10^6\ \mathrm{J\,kg^{-1}}$), q_1 is the surface specific humidity, q_2^* is the free-tropospheric saturation specific humidity, g is the planetary gravitational acceleration, and Z_a is the height of convection, which we take to be a constant.

We set the relative humidity of the dayside free troposphere, RH_2, to 80% and of the nightside free troposphere, RH_3, to 30%, roughly the mean values we obtain from CAM3 simulations over a variety of stellar fluxes. Similarly, we set the dayside boundary layer relative humidity, RH_1, to 90%. We calculate the height of convection, Z_a, by specifying the pressure of the free tropospheric layer, P_a, and assuming a scale height of 5000 m. This scale height is smaller than that of Earth, ≈7500 m, due to the fact that we use a larger gravitational acceleration (13.7 versus 9.8 $\mathrm{m\,s^{-2}}$).

A simple convective cloud scheme is employed to describe the cloud behavior. The effective cloud fraction (f_c) is related to the convective heat flux (F_c) with an upper limit of 1.0:

$$f_c = \min(k_3 \ln(F_c + 1.0), 1.0), \tag{13}$$

where k_3 is an adjustable parameter that we set to $k_3 = 0.08$ by tuning the model to roughly reproduce cloud albedos obtained in CAM3 simulations. This logarithmic scheme for convective clouds was proposed by Xu & Krueger (1991) and used to parameterize the cloud fraction in CAM3 (Collins et al. 2004) and its recently released versions, CAM4 (Neale et al. 2010b) and CAM5 (Neale et al. 2010a), and it is able to roughly simulate the convective cloud coverage over the tropics of Earth (Hack et al. 2006). We assume that the nightside column is cloud-free because clouds there can have no albedo effect and have a small greenhouse effect because they are near the surface.

Cloud albedo depends on both cloud fraction and cloud microphysics. For simplicity, detailed microphysical descriptions (Kitzmann et al. 2010; Zsom et al. 2012) are not included in the model, and we assume that the cloud albedo equals one where there are clouds. Using this assumption, the planetary albedo (α_p), determined by the combined effect of surface and cloud albedos, is

$$\alpha_p = 0.09 + f_c - 0.09 \times f_c, \tag{14}$$

where 0.09 is the albedo of seawater averaged over the dayside (including the dependence of albedo on the stellar zenith angle). If there are no clouds, the planetary albedo is equal to the seawater albedo. We do not include the contribution of sea ice and snow to the planetary albedo, which would only be relevant near the outer edge of the habitable zone when significant amounts of sea ice and snow spread to the dayside.

We specify the cloud emission temperature (T_c) to be a constant in accordance with the FAT hypothesis. We set $T_c = 230$ K, which is the value suggested by our GCM simulations

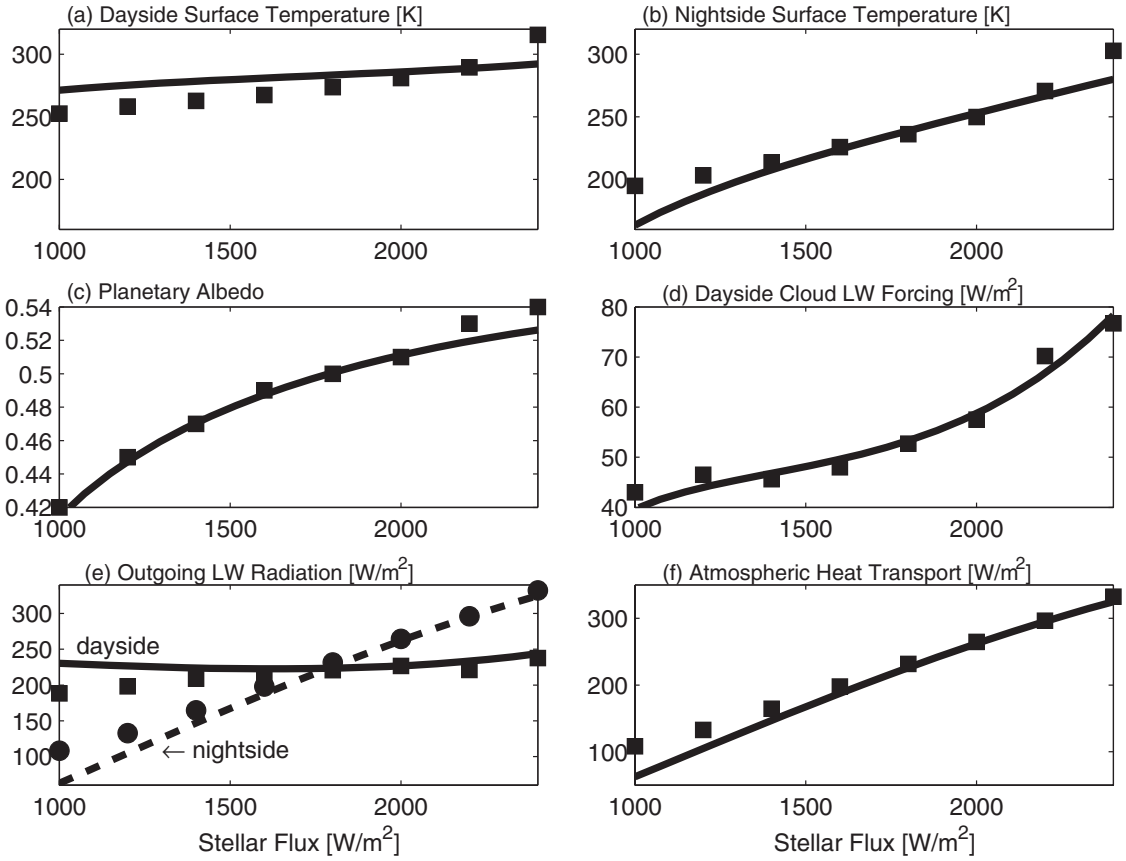

Figure 5. Reference climate solution of the two-column model as a function of stellar flux (S_0) compared with output from the GCM CAM3. Lines represent the results of the two-column model, and squares and circles represent those of the GCM CAM3. (a) Dayside surface temperature (T_1), (b) nightside surface temperature (T_4), (c) planetary albedo (α_p), (d) dayside cloud longwave forcing (C_l), (e) outgoing longwave radiation on the dayside (OLR_1) and on the nightside (OLR_2), and (f) atmospheric heat transport from dayside to nightside (F_a). Model parameters are listed in Table 1. The squares and circles in panel (e) are the same as those in Figure 4(b) for comparison.

(see Figure 3) and is 12 K higher than that of tropical anvil clouds of Earth (≈218 K; Houze & Betts 1981).

We neglect a variety of physical processes in the model. For example, we do not consider shortwave absorption by water vapor and clouds, feedbacks due to changes of convection depth and relative humidity, the detailed interaction between atmospheric and oceanic circulations, and the momentum and moisture budgets. Despite these simplifications, the low-order two-column model is able to capture many of the fundamental features of the GCM simulations.

4. REFERENCE CLIMATE AND MODEL SENSITIVITY

In this section, we first show that it is possible to tune the two-column model to reproduce the results of the GCM CAM3 simulations. Next, we investigate the sensitivity of the model to increases in ocean heat transport, cloud radiative forcing, and atmospheric emissivity.

4.1. Reference Climate

We plot model variables at steady state for the reference climate as a function of stellar flux in Figure 5 (see Table 1 for model parameters). The ocean heat transport is set to zero in these calculations. We choose the values of P_a, T_c, RH_1, RH_2, and RH_3 by averaging equivalent variables in the CAM3 GCM simulations. We then tune the two-column model to CAM3 by adjusting only three parameters: k_1, k_2, and k_3. When the two-column model is tuned to CAM3 in this way, it is able to capture the fundamental features of the climate, including surface temperature, planetary albedo, cloud longwave forcing, thermal emission flux, and atmospheric heat transport.

Both the dayside and nightside surface temperatures increase as the stellar flux increases, and their magnitudes are close to CAM3's. The planetary albedo of the two-column model behaves very similarly to that of CAM3, which shows that our simple convective cloud scheme is capable of capturing the bulk effects of cloud albedo on the climate. The planetary albedo of tidally locked terrestrial planets (between 0.42 and 0.54) is much higher than that of Earth (≈0.3). This results from a high cloud fraction near the substellar point, where the stellar flux is highest (YCA13). The two-column model also has very similar dayside cloud longwave forcing to that of CAM3 (between 40 and 80 W m^{-2}).

As the stellar flux increases, both models predict that the dayside thermal emission flux is nearly constant whereas the nightside thermal emission increases rapidly (Figure 5(e)). When the stellar flux is higher than ≈1800 W m^{-2}, the thermal emission flux on the nightside exceeds that on the dayside. The strength of atmospheric heat transport from dayside to nightside is quite similar between the two-column model and CAM3 (Figure 5(f)), confirming the accuracy of the WTG approximation.

Figure 5 shows that as the stellar flux increases, the nightside surface temperature increases much faster than the dayside

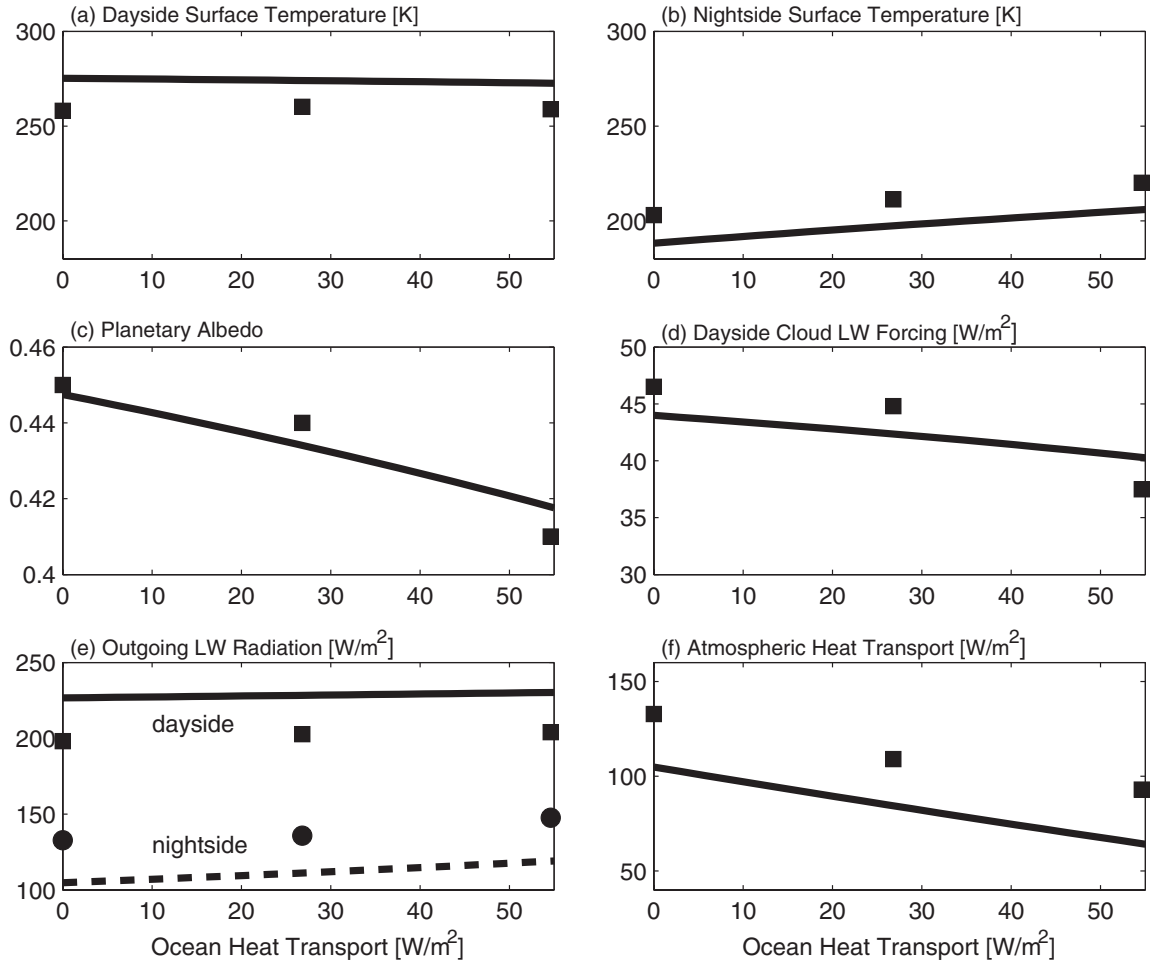

Figure 6. As in Figure 5, but as a function of ocean heat transport from dayside to nightside (F_o). The stellar flux is 1200 W m^{-2} in these calculations. Model parameters except for the parameter varied (F_o), are the same as those for the reference climate calculations (Table 1). The moderate differences between the two-column model and GCM are due to the difference in the base state with $F_o = 0$ (Figure 5), and can be removed by changing either the parameter k_1 or k_2 slightly.

surface temperature. The main reason for this is that the atmosphere efficiently transports energy absorbed on the dayside to the nightside (Figure 5(f)).

These comparisons between the two-column model and CAM3 demonstrate that despite of the simplicity of our assumptions, the two-column model is able, when appropriately tuned, to reproduce the main climate features of tidally locked terrestrial planets as simulated by a GCM. This indicates that the climate of tidally locked planets is well described by the handful of essential physical processes contained in the two-column model.

4.2. The Effect of Ocean Heat Transport

Here we investigate how the climate responds to imposed ocean heat transport from dayside to nightside. To investigate this we performed a series of calculations in which the ocean heat transport is varied while the stellar flux is fixed to a constant (Figure 6). As the ocean heat transport is increased, the dayside surface temperature decreases slightly while the nightside surface temperature increases significantly, so that the global-mean surface temperature increases, and the surface temperature and thermal emission contrasts between dayside and nightside decrease. Both the planetary albedo and the cloud longwave forcing decrease because increasing ocean heat transport decreases the day–night surface temperature contrast, weakening the convergence and convection on the dayside. The atmospheric heat transport decreases in response to the increase in ocean heat transport, such that the total heat transport shows a small increase. This compensation between the atmosphere and ocean is consistent with the results of simulations with a fully coupled 3D atmosphere–ocean circulation model (Hu & Yang 2014) and is similar to the behavior that meridional atmospheric and ocean heat transports on Earth are believed to exhibit (Stone 1978; Farneti & Vallis 2013).

We tuned the two-column model to the GCM over a range of stellar fluxes, and it deviates somewhat from the GCM when the ocean heat transport is zero at the particular stellar flux for which we varied the ocean heat transport in the GCM (Figure 6). Nevertheless, the two-column model does a good job of reproducing the trends of the GCM as the ocean heat transport is increased. Moreover, by slightly changing k_1 or k_2 we can greatly improve the match between the GCM and the two-column model when the ocean heat transport is varied at this particular stellar flux (not shown).

The fact that the two-column model can roughly reproduce the behavior of the GCM when ocean heat transport is varied, even though it was tuned to match the GCM when stellar flux is varied, suggests that the approximations we have made capture the relevant physics, rather than the model simply being cleverly tuned. For example, the fact that the response of atmospheric heat transport to changes in ocean heat transport in the

two-column model is very similar to that in the GCM emphasizes the validity of the WTG approximation. Furthermore, the similar changes in planetary albedo and cloud longwave forcing between the models suggests that the convective scheme and FAT hypothesis are faithful representations of the more complete physics contained in the GCM.

4.3. The Importance of Cloud Albedo Effect

Clouds have significant effects on the climate of tidally locked planets (YCA13). In order to further establish the importance of clouds, we performed calculations with either the cloud albedo or cloud longwave forcing set to zero (Figure 7). For the no cloud albedo effect experiment, Equation (14) is not used and the planetary albedo is set to equal to the seawater albedo (0.09). For the no cloud longwave effect experiment, Equation (13) is not used and the cloud longwave forcing is set to zero.

Comparisons with the reference climate experiments show that the global-mean surface temperature decreases by ≈15 K for the no cloud longwave effect experiments while it increases by ≈40 K if the cloud albedo effect is turned off. This indicates that the cloud albedo cooling effect is much stronger than the cloud greenhouse warming effect. The net effect of the clouds is therefore to cool the planet dramatically, delaying the onset of a runaway greenhouse, as addressed in YCA13.

We also performed a series of calculations with a fixed planetary albedo of 0.415 and a fixed cloud longwave forcing of 40 W m^{-2}, which are their values when the stellar flux is equal to 1000 W m^{-2}. These calculations investigate the model with clouds, but without a cloud feedback (changes in cloud forcing as a function of climate). The dashed line of Figure 7 shows that the surface temperature increases by ≈15 K on the dayside, relative to the interactive cloud case, when the stellar flux is 2400 W m^{-2}. The cloud albedo feedback therefore has a significant cooling effect on the planet.

4.4. The Importance of the Nightside Radiator Fin

Atmospheric emissivity affects the strength of the greenhouse effect and the efficiency of infrared energy loss to space. We perform a set of experiments to test the sensitivity of the climate to atmospheric emissivity. In these experiments, Equation (10) is not used, and instead atmospheric emissivity is set to a series of values from zero to one. The cloud radiative forcing is fixed in order to focus on the role of atmospheric emissivity.

Figure 8(a) shows the dayside surface temperature as a function of the dayside atmospheric emissivity (ε_2). In these experiments, the nightside atmospheric emissivity (ε_3) is fixed to 0.5. As ε_2 is increased, the dayside atmospheric greenhouse effect increases, and consequently the surface temperature increases. The magnitude of the increase, however, is small even when ε_2 is increased from zero to one. This is due to an increase in atmospheric heat export to the nightside (Figure 8(b)), which warms the nightside and weakens the increase in the dayside surface temperature.

Figure 8(c) shows the sensitivity of the climate to varying the nightside atmospheric emissivity (ε_3). In these experiments, the dayside atmospheric emissivity (ε_2) is fixed to 0.5. As ε_3 is increased, the dayside surface temperature decreases strongly, although the nightside and global-mean surface temperatures increase (not shown). As ε_3 is increased from zero to 1.0, the dayside surface temperature decreases by ≈45 K. As ε_3 is increased, the efficiency of the atmospheric infrared energy loss to space increases, which requires a great increase in atmospheric

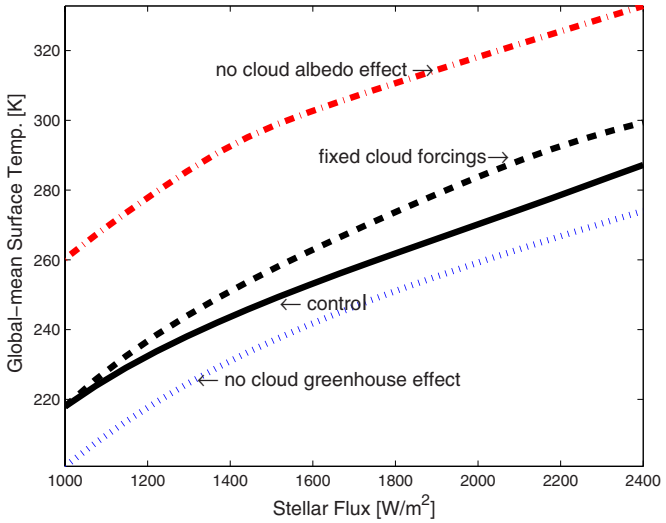

Figure 7. Sensitivity of global-mean surface temperature $(T_1 + T_4)/2$ to cloud albedo and cloud longwave forcing, as a function of stellar flux (S_0). Solid line: with both effects; dashed-dotted line: no cloud albedo effect ($\alpha_p = 0.09$); dotted line: no cloud greenhouse effect ($C_l = 0$); and dashed line: planetary albedo and cloud greenhouse effect are fixed to those at a stellar flux of 1000 W m^{-2} ($\alpha_p = 0.415$, $C_l = 40$ W m^{-2}; i.e., no cloud feedback). Other model parameters are the same as those for the reference climate calculations (Table 1).

(A color version of this figure is available in the online journal.)

heat transport from dayside to nightside (Figure 8(d)), therefore cooling the dayside surface.

We can draw an important physical lesson from these experiments: the nightside acts like a "radiator fin," similar to the subtropics of Earth (Pierrehumbert 1995), only more pronounced. All the stellar energy is deposited on the dayside and the water vapor and cloud greenhouse effects prevent the atmosphere from getting rid of all this energy locally. Much of the energy is instead transported by the atmosphere to the nightside where the air is dry, there is a strong temperature inversion, and the cloud greenhouse effect is negligible, so that infrared energy is easily emitted to space (as it would be by a "radiator fin"). The nightside atmosphere therefore has a stabilizing effect on the climate of the planet.

The radiator-fin effect cannot be captured in a single column model, even a one-dimensional (1D) radiative–convective model with an extremely sophisticated radiative transfer scheme, because it requires horizontal heat transport to connect the moist and dry regions. In order to demonstrate this, we construct a one-column model with the same parameters as the two-column model. A comparison of the surface temperature as a function of the stellar flux in the one-column and two-column models is shown in Figure 9. We find that the surface temperature of the one-column model is ≈15–30 K higher than the two-column model because the one-column model is not able to capture the effect of the radiator fin. The radiator-fin effect becomes weak at high stellar fluxes because the atmospheric emissivities of both the dayside and nightside approach one. This is a limitation of the simple radiative scheme in our model. Further investigation of the effect of the radiator fin on the runaway greenhouse will require a 2D or 3D model with a more sophisticated radiative scheme.

5. DAY–NIGHT THERMAL EMISSION CONTRAST

YCA13 proposed that cloud behavior on tidally locked terrestrial planets near the inner edge of the habitable zone

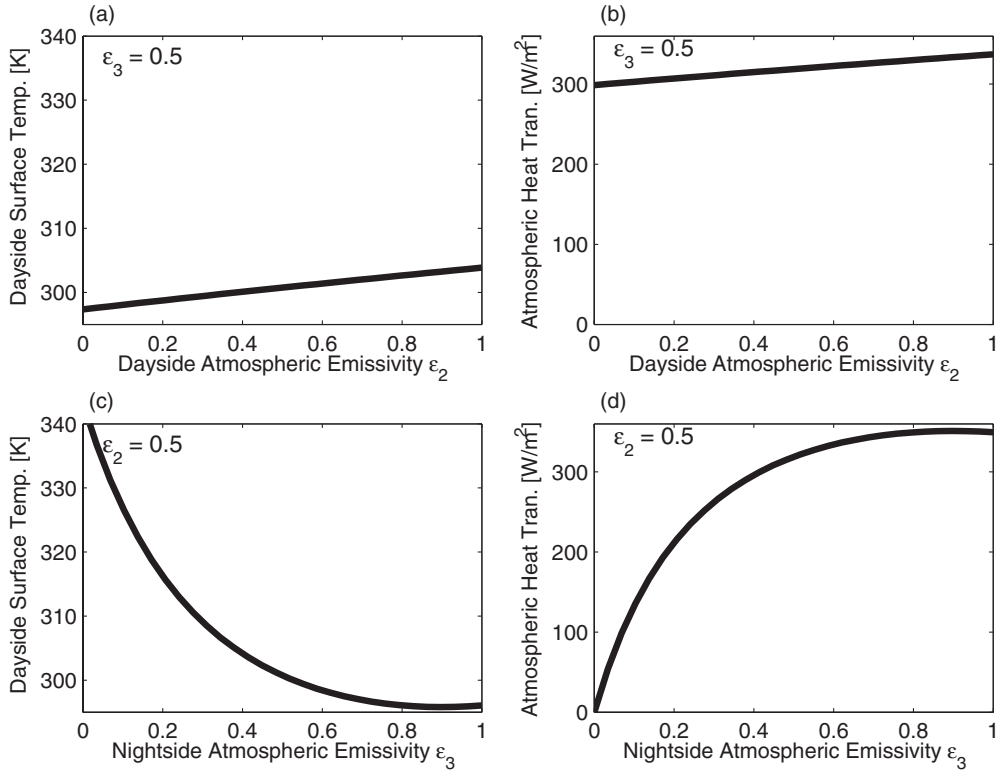

Figure 8. Sensitivity of the climate to atmospheric emissivity of dayside (ε_2) and nightside (ε_3). Left panels: dayside surface temperature (T_1); right panels: atmospheric heat transport from dayside to nightside (F_a). (a) and (b): varying ε_2 but fixed ε_3 to 0.5; (c) and (d): varying ε_3 but fixed ε_2 to 0.5. The stellar flux is 2400 W m^{-2}. Planetary albedo and cloud longwave forcing are fixed ($\alpha_p = 0.415$, $C_l = 40$ W m^{-2}). Other model parameters are the same as those for the reference climate calculations.

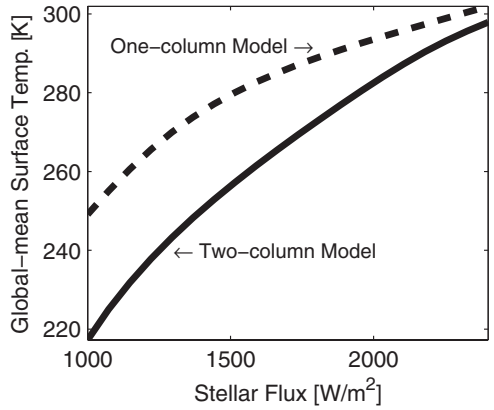

Figure 9. Effect of the radiator fin on the global-mean surface temperature. The one-column model (without the radiator fin) has the same parameters of the two-column model (including the radiator fin), including planetary albedo ($\alpha_p = 0.415$), cloud longwave forcing ($C_l = 40$ W m^{-2}), relative humidity, and atmospheric emissivity (Table 1).

would cause higher infrared thermal emission from the nightside than the dayside. This would lead to a reversal in the thermal phase curve, which is a qualitatively different signal than would normally be expected. In this section, we consider the difference in thermal emission flux between dayside and nightside in the two-column model, and show how basic physical parameters may affect this signal.

In a steady state, the dayside column heat budget can be obtained by summing Equations (2) and (3),

$$\frac{1}{2}S_0(1-\alpha_p) - F_a - F_o = \mathrm{OLR}_1. \quad (15)$$

OLR_1 is the thermal emission flux from the dayside, with

$$\mathrm{OLR}_1 = (1-\varepsilon_2)\sigma T_1^4 + \varepsilon_2\sigma T_2^4 - C_l, \quad (16)$$

where the sum of the first and second terms of the right hand side is the outgoing infrared emission in clear-sky conditions, and the third term is the reduction of the outgoing infrared emission due to the presence of clouds with

$$C_l = f_c\left((1-\varepsilon_2)\sigma T_1^4 + \varepsilon_2\sigma T_2^4\right) - f_c\sigma T_c^4. \quad (17)$$

Figure 10(a) shows the three terms of Equation (16) in the reference climate experiments. Surface emission reaching the top of the atmosphere decreases greatly with increasing stellar flux although the surface temperature increases. This is due to the increase of atmospheric absorption. Water vapor concentration increases rapidly with air temperature because of the strong temperature dependence of saturation water vapor pressure following the Clausius–Clapeyron relation, reducing the thermal emission to space. Emission by the atmosphere increases with increases in stellar flux due to increases of the air temperature (T_2) and atmospheric emissivity (ε_2). The cloud longwave effect decreases with increasing stellar flux, also reducing the thermal emission to space. The cloud effect is comparable to that of water vapor. Due to the combined effect of water vapor and clouds, the dayside OLR curve as a function of the stellar flux is very flat. Figure 10(a) also shows that if the stellar flux is low, the optical depth of the atmosphere is small, and OLR_1 is close to the unmodified upward radiation from the surface. If the stellar flux is high, the surface upward emission is blocked by the optically thick atmosphere, and the outgoing thermal emission is primarily determined by the upper tropospheric temperature.

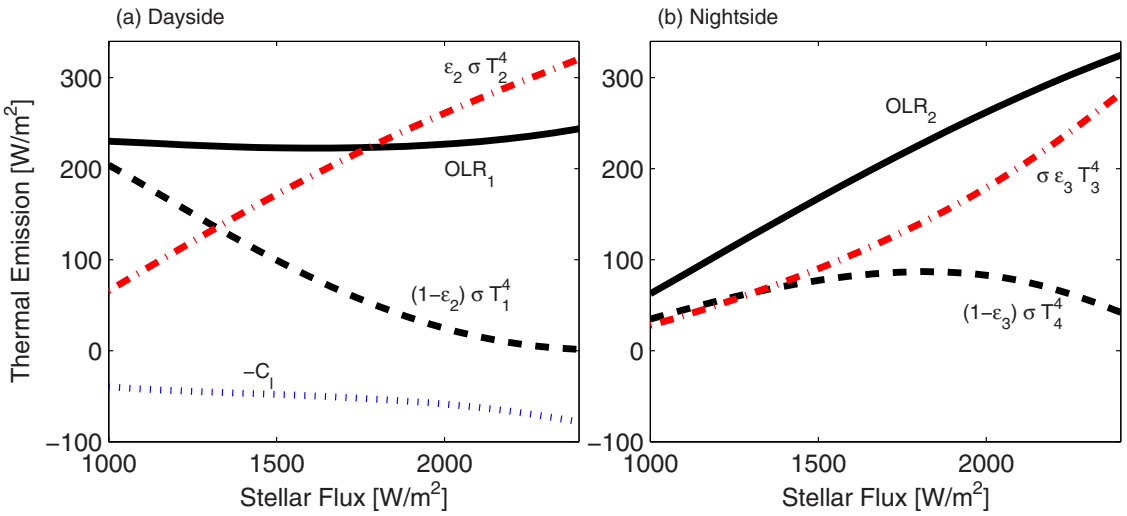

Figure 10. (a) Dayside and (b) nightside thermal emission fluxes as a function of the stellar flux (S_0) between 1000 and 2400 W m^{-2}. Solid line: thermal emission flux to space, which has to be equal to the sum of other terms (see Equations (16) and (19)); dashed line: surface upward emission minus the absorption by water vapor; dashed–dotted line: atmospheric reemission; and dotted line: the effect of clouds. Model parameters are the same as those for the reference climate calculations (Table 1).

(A color version of this figure is available in the online journal.)

For the thermal emission flux on the dry nightside, water vapor has a small effect, and low-level clouds there have nearly zero effect. The nightside column heat budget can be obtained by summing Equations (4) and (5),

$$F_a + F_o = \mathrm{OLR}_2, \tag{18}$$

where OLR_2 is the thermal emission flux to space:

$$\mathrm{OLR}_2 = (1-\varepsilon_3)\sigma T_4^4 + \varepsilon_3 \sigma T_3^4. \tag{19}$$

This means that the thermal emission flux on the nightside is equal to the sum of heat transports from the dayside by the atmosphere and ocean. Figure 10(b) shows the two terms of OLR_2 as a function of stellar flux. As the stellar flux increases, surface emission reaching the top of the atmosphere first increases due to the increase in surface temperature, and then decreases due to the increase of water vapor absorption. Atmospheric emission increases with increasing stellar flux due to increases of air temperature and emissivity. The net effect of the two terms is a strong increase in the thermal emission flux with increasing stellar flux.

If we assume a saturated atmosphere on the dayside, there will exist an upper limit for OLR_1 at which the atmosphere becomes optically thick at all infrared wavelengths (Kasting et al. 1993). The limit is ≈280 W m^{-2} for planets with pure water atmospheres, Earth's gravity, and no clouds (Goldblatt et al. 2013). If clouds are further considered, the limit will be lower. On the nightside, thermal infrared energy is more easily emitted to space through the radiator fin.

A remaining question is: what is the critical stellar flux (S_c) at which the dayside outgoing thermal emission flux becomes equal to or less than that of the nightside, i.e., $\mathrm{OLR}_1 \leqslant \mathrm{OLR}_2$? If OLR_1 is higher than OLR_2, the phase curve maximum should occur when the dayside of the planet is facing the observer. If OLR_1 is lower than OLR_2, the phase curve maximum should occur when the nightside is facing the observer. This striking, qualitative reversal in the thermal phase curve would be strong evidence for the Earth-like cloud behavior, if observed. Because of this, it is important to understand which model parameters exert the strongest control on S_c.

In Figure 11, we show how S_c changes as we vary k_1, k_2, k_3, T_c, P_a, and F_o, which are the most important independent parameters of the model. Here, k_1 represents the strength of adiabatic warming on the nightside surface due to large-scale dry descent (Equation (9)); k_2 is a coefficient relating water vapor to the infrared opacity (Equation (10)); k_3 is a constant that relates the strength of convection to the cloud fraction (Equation (13)); T_c is the cloud emission temperature; P_a is the depth of convection; F_o is the strength of ocean heat transport.

Changing k_1, P_a, and F_o does not influence the value of S_c very much (Figure 11). In contrast, k_2, k_3, and T_c strongly influence S_c. Increasing k_2 increases the optical thickness due to water vapor. Since there is more water vapor on the dayside, this preferentially decreases OLR_1, and therefore decreases S_c. Although k_2 is a necessary parameter in the two-column model, models with a more sophisticated radiative transfer scheme should agree on water vapor emissivity, and therefore the processes represented by k_2 are unlikely to be a major source of uncertainty in S_c.

The effects of k_3 and T_c on S_c are more likely to be relevant for future studies. These parameters represent cloud processes, which can differ significantly between complicated climate models. Increasing the cloud emission temperature (T_c) decreases the strength of cloud longwave forcing, increasing OLR_1 and therefore increasing S_c. Increasing k_3 causes an increase in the cloud fraction for a given convective heat flux, which increases both the cloud albedo and the cloud longwave forcing. Because the cloud albedo cooling effect is always stronger than the cloud greenhouse warming effect, water vapor amount and consequently atmospheric emissivity decrease. Since this primarily increases the OLR on the dayside, increasing k_3 causes S_c to increase. Cloud behavior will therefore be critical for determining the critical stellar flux (S_c), and a measurement of S_c will help us distinguish between different cloud models.

Finally we note that other factors that we have not explicitly included in the two-column model, such as atmospheric CO_2,

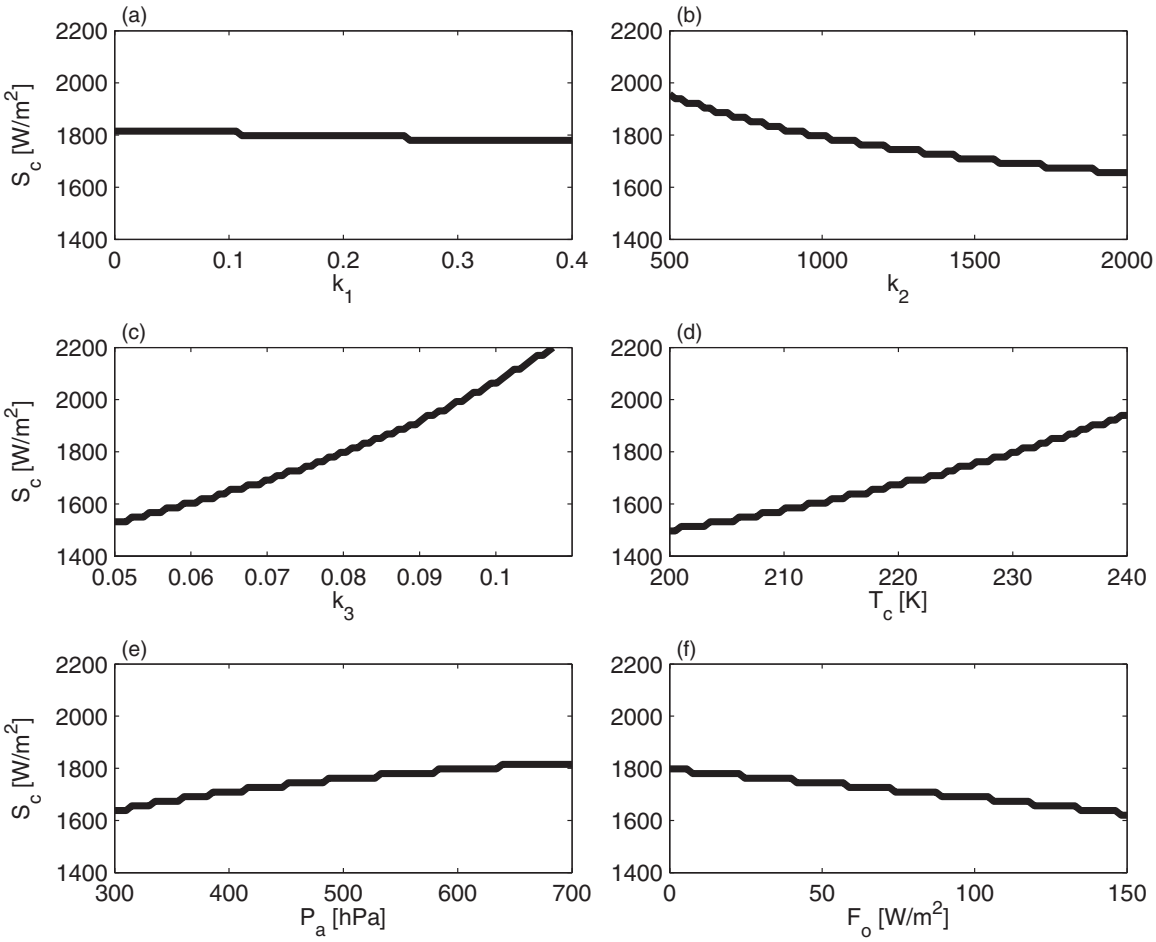

Figure 11. Critical stellar flux (S_c) at which the thermal emission flux of the dayside becomes equal to or less than that of the nightside ($OLR_1 \leqslant OLR_2$), as a function of (a) k_1, a parameter in Equation (9), representing the strength of adiabatic heating on the nightside surface due to large-scale dry descent; (b) k_2, a parameter in Equation (10), representing the strength of water vapor absorption; (c) k_3, a parameter in Equation (13), representing the increase in cloud fraction when the convective heat flux increases; (d) T_c, the cloud emission temperature; (e) P_a, the depth of convection; and (f) F_o, the ocean heat transport. Model parameters, except for the parameter varied, are the same as those for the reference climate calculations (Table 1).

can influence the day–night emission contrast. For example, simulations in CAM3 show that increasing the CO_2 concentration strengthens the day–night thermal emission contrast because it weakens the nightside inversion and leads to a stronger water vapor feedback on the warmer dayside (not shown). This can change the critical stellar flux by ≈400 W m^{-2} when the CO_2 concentration is increased from 0 to 0.1 bar, so that large uncertainties in the CO_2 of an observed planet would make it harder to fit a cloud model to the observed thermal emission contrast.

6. CONCLUSIONS

We constructed a low-order two-column model to simulate the climate of tidally locked terrestrial planets near the inner edge of the habitable zone of M-dwarf stars. This model incorporates the WTG approximation to calculate horizontal atmospheric heat transport, the FAT hypothesis to calculate the cloud longwave effect, and a simple convective cloud scheme to calculate the cloud albedo. Our main findings are as follows:

1. The relatively few parameters of the two-column model can be tuned to reproduce the basic behavior of a very complicated global climate model and respond faithfully to variations in both the stellar flux and ocean heat transport. This suggests that the physical processes built into the two-column model are the most important ones for determining the climate of tidally locked terrestrial planets.
2. The two-column model clearly illustrates the importance of dayside clouds and a nightside "radiator fin" for determining the climate of tidally locked planets. Dayside clouds increase the planetary albedo, which cools the planet and delays the onset of a runaway greenhouse. The radiator fin, primarily maintained by the dryness of the atmosphere and the temperature inversion on the nightside, allows the planet to easily lose energy to space through infrared thermal emission, which also cools the planet. Atmospheric dynamics are crucial for both of these effects, so they cannot be calculated by 1D radiative–convective models. This means that 1D radiative–convective models will tend to produce overly conservative estimates of the inner edge of the habitable zone.
3. Observations of the day–night thermal emission contrast will be critical for deciphering the climate of tidally locked terrestrial planets. As the stellar flux increases, nightside emission increases faster than dayside emission, so that at a critical stellar flux there will be a reversal in the day–night thermal emission contrast, with higher emission from the nightside. Sensitivity experiments in the two-column model show that cloud variables are most likely to cause differences in the critical stellar flux between

different models. This means that future observations of the day–night thermal emission contrast will be useful for distinguishing between cloud models.

We are grateful to Daniel D. B. Koll, Feng Ding, Yuwei Wang, and Feng Tian for helpful discussions and comments. D.S.A. acknowledges support from an Alfred P. Sloan Research Fellowship. We also thank two anonymous reviewers for their constructive comments.

REFERENCES

Abbot, D. S., & Tziperman, E. 2009, JAtS, 66, 519
Clement, A. C., & Seager, R. 1999, JCli, 12, 3384
Collins, W. D., Basch, P. J., Boville, B. A., et al. 2004, Technical Note, Document NCAR-TN-464+STR (Boulder, CO: NCAR)
Donohoe, A., & Battisti, D. S. 2011, JCli, 24, 4402
Edson, A., Lee, S., Pollard, D., Bannon, P. R., & Kasting, J. F. 2011, Icar, 212, 1
Emanuel, K. 1994, Atmospheric Convection (New York: Oxford Univ. Press)
Emanuel, K. 2002, JGR, 107, 4077
Farneti, R., & Vallis, G. K. 2013, JCli, 26, 7151
Goldblatt, C., Robinson, T. D., Zahnle, K. J., & Crisp, D. 2013, NatGe, 6, 661
Hack, J. J., Caron, J. M., Yeager, S. G., et al. 2006, JCli, 19, 2199
Hartmann, D. L., & Larson, K. 2002, GeoRL, 29, 1951
Hartmann, D. L., & Michelsen, M. L. 1993, JCli, 6, 2049
Heng, K., & Vogt, S. S. 2011, MNRAS, 415, 2145
Houze, R. A., & Betts, A. K., Jr. 1981, RvGeo, 19, 541
Hu, Y., & Ding, F. 2011, A&A, 526, A135
Hu, Y., & Yang, J. 2014, PNAS, 111, 629
Joshi, M. M. 2003, Asbio, 3, 415
Joshi, M. M., Haberle, R. M., & Reynolds, R. T. 1997, Icar, 129, 450
Kasting, J. F., Whitmire, D. P., & Reynolds, R. T. 1993, Icar, 101, 108
Kitzmann, D., Patzer, A. B. C., vonParis, P., et al. 2010, A&A, 511, A66
Knutson, H. A., Charbonneau, D., Allen, L. E., et al. 2007, Natur, 447, 183
Kopparapu, R. K., Ramirez, R., Kasting, J. F., et al. 2013, ApJ, 767, 131
Kuang, Z., & Hartmann, D. L. 2007, JCli, 20, 2051
Larson, K., Hartmann, D. L., & Klein, S. A. 1999, JCli, 12, 2359
Leconte, J., Forget, F., Charnay, B., et al. 2013, A&A, 554, A69
Li, Y., Yang, P., North, G. R., & Dessler, A. 2012, JAtS, 69, 2317
Merlis, T. M., & Schneider, T. 2010, JAMES, 2, 13
Mills, S. M., & Abbot, D. S. 2013, ApJL, 774, L17
Neale, R. B., Chen, C.-C., Gettelman, A., et al. 2010a, Technical Note, Document NCAR-TN-486+STR (Boulder, CO: NCAR)
Neale, R. B., Richter, J. H., Conley, A. J., et al. 2010b, Technical Note, Document NCAR-TN-485+STR (Boulder, CO: NCAR)
Perez-Becker, D., & Showman, A. P. 2013, ApJ, 776, 134
Pierrehumbert, R. T. 1995, JAtS, 52, 1784
Pierrehumbert, R. T. 2010, Principles of Planetary Climate (Cambridge: Cambridge Univ. Press)
Pierrehumbert, R. T. 2011, ApJL, 726, L8
Ramanathan, V., Cess, R. D., Harrison, E. F., et al. 1989, Sci, 243, 57
Ramanathan, V., & Collins, W. 1991, Natur, 351, 27
Raymond, D. J. 1995, JAtS, 55, 3945
Shields, A. L., Meadows, V. S., Bitz, C. M., et al. 2013, Asbio, 13, 715
Showman, A. P., & Polvani, L. M. 2011, ApJ, 738, 71
Showman, A. P., Wordsworth, R. D., Merlis, T. M., & Kaspi, Y. 2013, in Comparative Climatology of Terrestrial Planets, ed. S. J. Mackwell et al. (Tucson, AZ: Univ. of Arizona Press), 277
Slingo, J. M. 1980, QJRMS, 106, 747
Sobel, A. H., Nilsson, J., & Polvani, L. M. 2001, JCli, 58, 3650
Stone, P. H. 1978, DyAtO, 2, 123
Tarter, J. C., Backus, P. R., Mancinelli, R. L., et al. 2007, Asbio, 7, 30
Wordsworth, R. D., Forget, F., Selsis, F., et al. 2010, A&A, 522, A22
Wordsworth, R. D., Forget, F., Selsis, F., et al. 2011, ApJL, 73, L48
Xu, K., & Emanuel, K. A. 1989, MWRv, 117, 1471
Xu, K. M., & Krueger, S. K. 1991, MWRv, 119, 342
Yang, J., Cowan, N. B., & Abbot, D. S. 2013, ApJL, 771, L45
Zelinka, M. D., & Hartmann, D. L. 2010, JGR, 115, D16117
Zsom, A., Kaltenegger, L., & Goldblatt, C. 2012, Icar, 221, 603